Fully Integrated Organic Nanocrystal Diode as High Performance Room Temperature NO_2 Sensor

Abdur Rehman Jalil, Hao Chang, Vineeth Kumar Bandari, Peter Robaschik, Jian Zhang, Pablo F. Siles, Guodong Li, Danilo Bürger, Daniel Grimm, Xingyuan Liu, Georgeta Salvan, Dietrich R. T. Zahn, Feng Zhu, Haibo Wang,* Donghang Yan, and Oliver G. Schmidt**

In the past decade, organic semiconductor materials have become promising candidates for gas sensors due to their high sensitivity, low production costs, and multiple function integration.[1–10] The reversible noncovalent bond interaction between organic semiconductors and gas molecules causes organic materials to be more suitable than inorganic materials for detecting toxic gas such as nitrogen dioxide (NO_2), sulfur dioxide (SO_2), or ammonia (NH_3) at room temperature (RT), which is of great importance for operation in complex and often hazardous gaseous environment.[11–13] This interaction process leads to a change in the mobile carrier density in the conductive channels of a diode or transistor device, eventually resulting in the variation of the output signal. For RT gas sensors, normally a thicker organic active layer provides more sensitive medium and hence a more stable electrical signal. However, disordered surfaces, pinholes, deep traps, and crystal domain boundaries in organic films render the gas diffusion and scattering complicated, and substantially decrease the gas absorption–desorption efficiency.[2] At present, the slow response-recovery process is the major challenge in RT organic gas sensors. For example, the recovery time of NO_2 sensors is slow—in the range of 1 h[14–17] and therefore still unpractical for applications.

Ordered organic nanostructures are regarded as ideal sensing channels to improve the absorption–desorption process in organic gas sensors.[12,15,18] The neat and compact channels with high surface-to-volume ratio can effectively expand the contact area for sensing analytes and reduce the remaining number of gas molecules in the bulk part of the active layer. Single-crystal molecular nanowires, ordered antenna structures, nanofiber networks, and structured ultrathin films have been employed in sensor devices to push the limits of low-ppm concentration gas detection and/or shorten the recovery time of the sensor device.[15,16,19–23] These results indicate that the gas sensor performance can be improved toward the extreme limit of high sensitivity and fast recovery if ordered nanoscale molecular structures are efficiently utilized as sensing medium.

However, full integration of nanoscale molecular structures with reliable electrical contacts has remained a persistent challenge in device fabrication procedures.[24–26] Difficulties from several aspects need to be tackled. For instance, for a vertical device geometry, simple evaporation of metal films to form top electrodes can easily harm the integrity of the molecular nanostructure and cause short circuits across the device. For a planar device geometry, accurate alignment of fine contacts with respect to single organic nanostructures is technologically challenging. Moreover, due to the low electron density in organic semiconductors, difficulties in forming low ohmic contacts limit the gas sensing process and reduce device sensitivity. Therefore, to create molecular nanostructure devices, high-yield fabrication procedures for robust contacts between metal electrodes and organic active layers are desperately sought-after. Recently, several novel approaches have been reported in this field and are expected to be applicable to a wide range of organic and hybrid systems.[27,28] One of these fabrication techniques for reliable vertical contacts relies on a previous publication by part of us, in which transport through a hybrid organic/inorganic molecular heterojunction was reported.[28]

Here, we report the full integration of a vertical organic nanocrystal diode and demonstrate its application in efficient NO_2 gas detection at RT. An organic nanopyramid structure

A. R. Jalil, V. K. Bandari, Dr. P. F. Siles, Dr. G. Li, Dr. D. Bürger, Dr. D. Grimm, Dr. F. Zhu, Prof. O. G. Schmidt
Material Systems for Nanoelectronics
Technische Universität Chemnitz
09107 Chemnitz, Germany
E-mail: f.zhu@ifw-dresden.de; o.schmidt@ifw-dresden.de

A. R. Jalil, V. K. Bandari, Dr. P. F. Siles, Dr. G. Li, Dr. D. Bürger, Dr. D. Grimm, Dr. F. Zhu, Prof. O. G. Schmidt
Institute for Integrative Nanosciences
IFW Dresden
01069 Dresden, Germany

H. Chang, Dr. H. Wang, Prof. D. Yan
Changchun Institute of Applied Chemistry
Chinese Academy of Sciences
130022 Changchun, China
E-mail: wanghb@ciac.jl.cn

P. Robaschik, Prof. G. Salvan, Prof. D. R. T. Zahn
Semiconductor Physics
Technische Universität Chemnitz
09107 Chemnitz, Germany

Dr. J. Zhang, Prof. X. Liu
Changchun Institute of Optics
Fine Mechanics and Physics
Chinese Academy of Sciences
130033 Changchun, China

Dr. G. Li, Prof. O. G. Schmidt
Center for Advancing Electronics Dresden
Dresden University of Technology
01062 Dresden, Germany

DOI: 10.1002/adma.201506293

ADVANCED MATERIALS
www.advmat.de

www.MaterialsViews.com

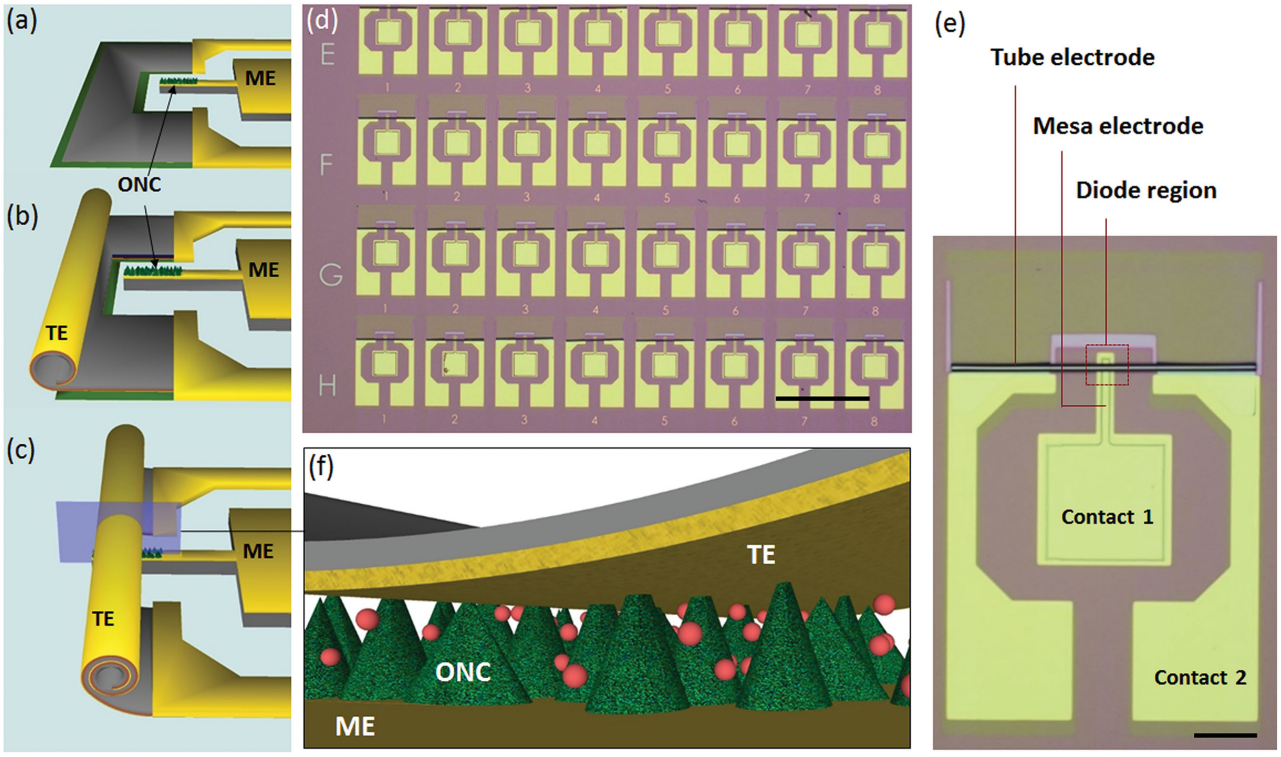

Figure 1. Structure of organic nanocrystal diode. The major fabrication steps for forming a robust top contact are shown in (a)–(c). Upon decomposition of the sacrificial layer (green part on substrate), the metal nanomembrane rolls up and smoothly contacts the top of the mesa structure. ME denotes mesa electrode; TE denotes tube electrode; ONC denotes organic nanocrystal. d) Micrograph of the large area gas sensor device array. Scale bar is 400 μm. A typical single device is magnified and shown in (e), in which the scale bar is 50 μm. f) Conceptual picture of cross section of tube/organic/mesa structure. VOPc nano-pyramids (green cones) provide sufficient space for NO_2 gas molecules to penetrate the structure. The red particles denote NO_2 gas molecules.

consisting of vanadyl phthalocyanine (VOPc) is sandwiched between a flat Au substrate electrode and a robust smooth Au top contact made by rolled-up metal nanomembranes. In this nanoscale diode, the VOPc crystalline nanopyramids act as functional units to detect NO_2, and efficient charge transfer from an organic heterojunction is employed to improve the contact resistance between the nanostructures and the electrodes. In this way, both a highly sensitive response to NO_2 molecules and a fast recovery of the sensor are achieved at the same time.

The major route for organic nanocrystal diode fabrication is shown in **Figure 1**a–c. First, on a finger-shaped mesa structure, which is about 10 μm wide and 400 nm high, a smooth 50 nm-Au layer is deposited to form the bottom electrode. A patterned area consisting of oxidized Ge and Au/Ti/Cr nanomembranes is formed as sacrificial layer and top electrode, respectively. Then, the organic nanocrystal layer is grown on the finger-shaped mesa Au electrode by organic molecular beam deposition. Upon selectively etching away the underlying sacrificial layer, the predefined strain-engineered metallic nanomembrane starts to detach from the substrate and rolls up onto the top of the mesa structure to contact the organic layer, hence forming a Metal/Organic/Metal diode. A more detailed description of the fabrication method and device components is provided in the Supporting Information and previous reports.[28–30] By applying in parallel the self-rolling and semiconductor micro-patterning techniques, an integrative chip is obtained where the organic nanocrystal diodes constitute a compact device array. Figure 1d shows the microscope image of the array, demonstrating the high reproducibility of the device fabrication with a yield of more than 95%. The rolled-up tubes are formed homogeneously and the average diameter is about 4 μm. Each contact pad (100 μm × 100 μm) is used for bonding Au lead wires to connect the devices with external circuitry. Figure 1f shows the concept image of the nanoscale organic diode, in which molecular nanostructures are sandwiched between the rolled-up nanomembrane electrode and the bottom plane electrode. NO_2 gas molecules can effectively pass through the gaps between the organic nanopyramid structures.

Highly sensitive and selective NO_2 sensors, based on metal phthalocyanines materials, have been demonstrated previously.[31,32] One of this class of materials, VOPc, is selected to construct the sensing channel in this work (**Figure 2**a). VOPc is highly sensitive to NO_2 owing to the redox process between phthalocyanine and NO_2 molecules, in which mobile hole carriers are generated and increase the film conductivity.[16,17] VOPc molecules can form polycrystalline films on different substrates, e.g. metal substrates, oxide substrates, self-assembled modifying layers, and conjugated molecule layers. VOPc shows different growth modes, and by carefully tuning the growth conditions the charge carrier transport properties can be controlled.[33] However, apart from the mobility of the

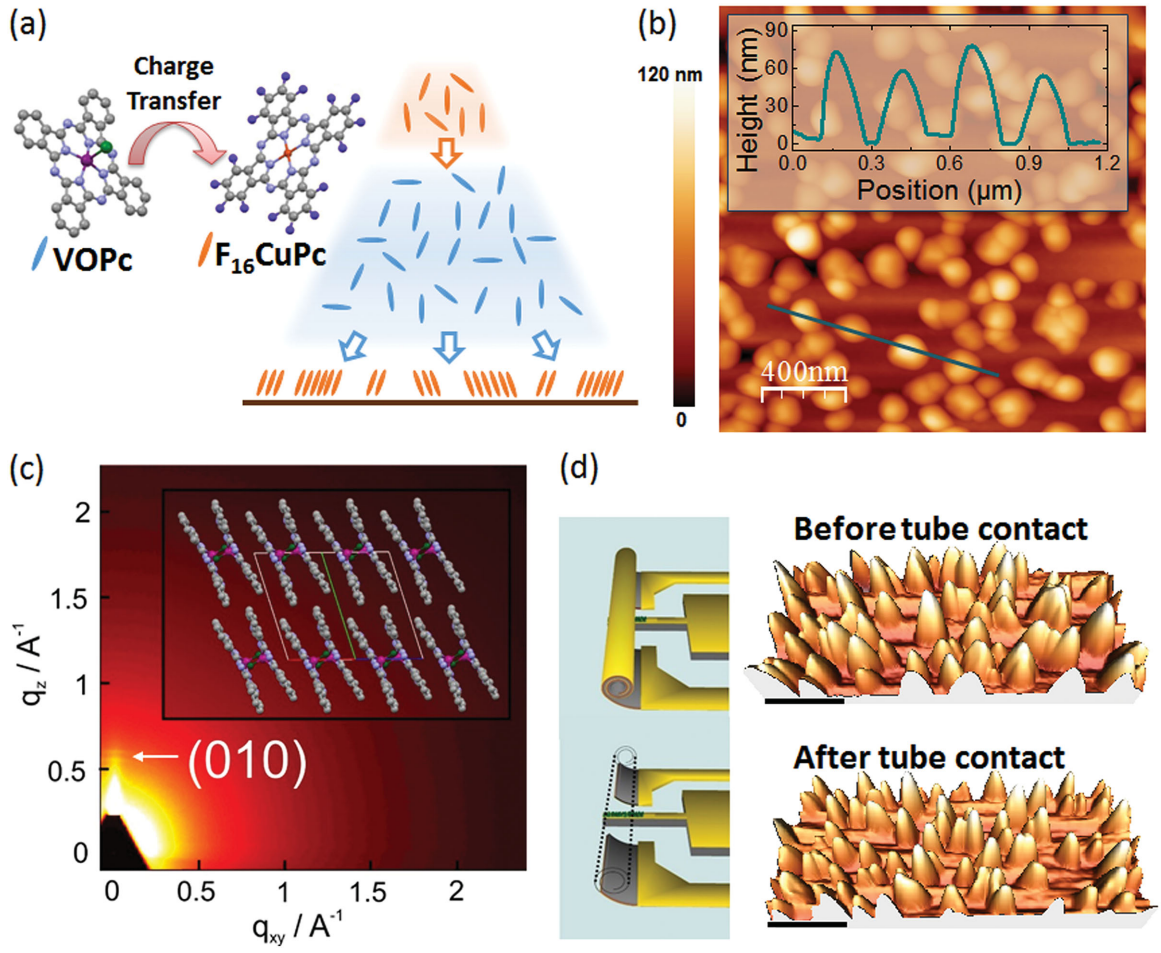

Figure 2. Morphology and structure of organic nanostructure. a) Molecular structure of VOPc and F_{16}CuPc, right panel shows the growing sequence. b) AFM of VOPc nanopyramids with F_{16}CuPc buffer layers. c) GIXD pattern of nanopyramids, the inset depicts the VOPc molecule packing. d) 3D topography demonstrates the morphology of nanopyramids before and after the contact by rolled-up tube. Scale bars are 400 nm.

molecular film, which is tightly connected to the film morphology and crystalline quality, the diode device performance crucially depends on the contact properties between film and electrode material. For the contact between a phthalocyanine molecular film and an Au electrode, an interfacial dipole forms when the Fermi energy levels align across the junction.[34,35] As a result, the energy barrier suppresses hole injection from the Au electrode to the VOPc. To solve this well-known problem in organic devices, two buffer layers are used to improve carrier injection by growing very thin layers (equivalent thickness: 0.5 nm each) of an n-type organic semiconductor material, copper hexadecafluoro-phthalocyanine (F_{16}CuPc), before and after deposition of the thick VOPc active layer (10 nm), as shown in Figure 2a. Due to the charge transfer effect, electrons will be transferred from F_{16}CuPc to VOPc and, as a result, electrons and holes accumulate in the F_{16}CuPc and VOPc material, respectively.[36–39] In such highly conductive heterostructures, hole injection from the Au electrode into the VOPc is significantly improved. During the formation of the VOPc layer sandwiched by the two F_{16}CuPc buffer layers, the substrate temperature is kept at 100 °C to provide the conditions for the formation of VOPc nanopyramids.[16] The morphology of such a film is characterized by atomic force microscopy (AFM) and the gibbous shape is clearly revealed in Figure 2b. As shown in the cross section (inset in Figure 2b) the molecular pyramids are around 50–100 nm high, and have a triangle-like profile with a bottom width of around 100–200 nm.

In order to identify the crystalline structure of the nanopyramids which consist of VOPc and the thin F_{16}CuPc buffer layers, 2D grazing incidence X-ray diffraction (2D-GIXD) was performed. As shown in Figure 2c, a diffraction spot appears near 0.60 $Å^{-1}$ in the out-of-plane direction (q_z), which corresponds to the VOPc (010) phase II triclinic crystal structure.[33] The diffraction pattern of F_{16}CuPc is not observed due to its small overall concentration in the organic layer. The nanopyramid structure does not cover the surface uniformly. Therefore, the diffraction from crystal planes other than (010) becomes very weak and is not observed in 2D-GIXD measurements. These results indicate that VOPc molecules adopt an edge-on configuration to form the nanopyramid crystalline structure as outlined in the inset of Figure 2c.[33]

In the last step of the diode fabrication, a strain-engineered Au/Ti/Cr multilayer nanomembrane is detached from the substrate and curls up upon gradual dissolution of the sacrificial

layer. Finally, the rolled-up tube electrode contacts the top of the nanopyramid structure and the diode fabrication is completed (Figure 1a–c). Whether and how the tube contacting process influences the morphology of the organic layer is an important factor for the device structure and properties. A simple experiment was performed to characterize the organic layer morphology after tube contacting. As shown in the left panel of Figure 2d, first the tube was brought in contact with the organic layer and was maintained at the same position for more than 24 h. Afterward the tube was carefully removed by microprobes. The right panel of Figure 2d shows the 3D topography of the organic nanopyramid structure before and after tube contacting. There is no obvious difference between the two morphologies, which indicates that the crystalline nanopyramids are sufficiently robust to withstand any detrimental effects by the roll-up of the nanomembrane. Hence, the nanopyramid structure preserves well after forming an intimate contact with the tube electrode, thus providing effective channels for detecting NO_2 and enough space for gas flow penetration.

Current–voltage (I–V) measurements were performed to characterize the fundamental electronic properties of an organic nanocrystal diode with F_{16}CuPc buffer layers (Device 1), in which the Au mesa (finger) electrode is set as ground (lower inset of **Figure 3**a). For comparison, one diode consisting of pristine VOPc nanopyramids without the F_{16}CuPc buffer layers

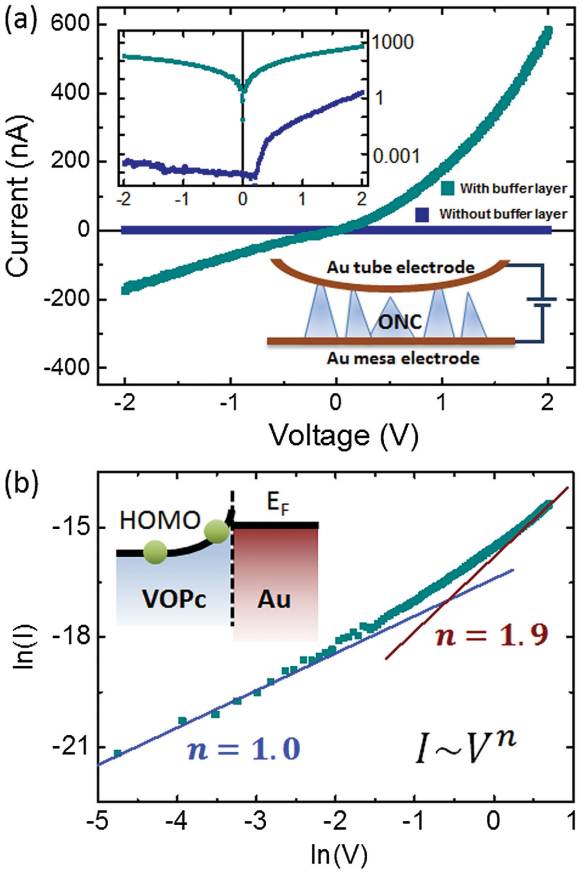

Figure 3. Electric transport properties of organic nanocrystal diodes. a) Schematic diagram of device structure and current–voltage curve with/without F_{16}CuPc buffer layers. b) Analysis of transport in ln$I$–ln$V$ scale.

was also prepared and measured (Device 2). According to the transport properties of VOPc films, holes dominate the transport because the Fermi level of the two Au electrodes is near to the VOPc's highest occupied molecular orbital.[40–42] Under positive bias, holes are injected from the Au tube electrode into the nanocrystals, whereas under negative bias the injection takes place from the Au mesa electrode. The measurement was performed from −2 V to +2 V. As shown in Figure 3, the diode without the heterojunction layer (without the buffer layers) shows much poorer conductivity compared to the diode with the F_{16}CuPc heterojunction layer, the difference of which can be as high as three orders of magnitude in current flow in the positive bias region (top inset of Figure 3a). This result agrees with previous similar reports and demonstrates that the efficient charge transfer effect between F_{16}CuPc and VOPc massively improves the carrier injection both from the Au tube and mesa electrodes.[36,43–45] For both nanocrystal diodes the I–V curves are not symmetric. The better transport ability under positive bias indicates that holes are preferably injected from the Au tube electrode into the nanocrystals, which is particularly pronounced in the device without F_{16}CuPc (upper inset of Figure 3a). In the microstructure design, the mesa electrode is about 400-nm higher than the tube electrodes' fixed terminals. When the nanomembranes roll up onto the top of the mesa structure a robust and tight contact between the tube and the molecules is generated.[28] Compared to the bottom contact area, the tube contact on top of the pyramids results in a much smaller injection area, even if the peaks of the nanopyramids are slightly truncated by the tube attachment. Assuming an 80-nm-high nanopyramid, a radius of the bottom and top interface area of 80 and 10 nm, respectively, the bottom contact area is almost two orders of magnitude larger than the top contact area. Therefore, the intimate mechanical contact between the robust rolled-up metal nanomembrane and the crystalline molecular clusters is greatly beneficial for carrier injection, although its contact area is much smaller compared to normal metal contacts to organic layers.

Since the electronic process plays an important role in detecting analyte gases, the charge transport mechanism needs to be investigated for determining the optimized function mode and working region of the sensor. Figure 3b shows the ln$I$–ln$V$ graph under positive bias for the organic nanocrystal diode incorporating the F_{16}CuPc heterojunction. Below 0.1 V, the slope of 1.0 indicates an ohmic current is generated under a low electric field (less than 1.0×10^4 V cm^{-1}), which confirms the good ohmic contact established in this nanocrystal diode. For bias larger than 1.5 V, a slope close to 2.0 indicates that subject to a high electric field (more than 1.5×10^5 V cm^{-1}) the transport is governed by the Mott–Gurney Law, and a space charge limited current (SCLC) is generated (in which I is directly proportional to V^2).[46,47] The transport properties under positive bias demonstrate that for the organic F_{16}CuPc/VOPc/F_{16}CuPc nanocrystal diode hole injection through the tube electrode and collection by the mesa electrode are efficient and are comparable to those of an ideal crystal.

One advantage of the nanoscale diode is that for reasonably high electric fields, the corresponding voltage applied to the device can be very small compared to the transport in planar configurations. The ohmic current region of Device 1

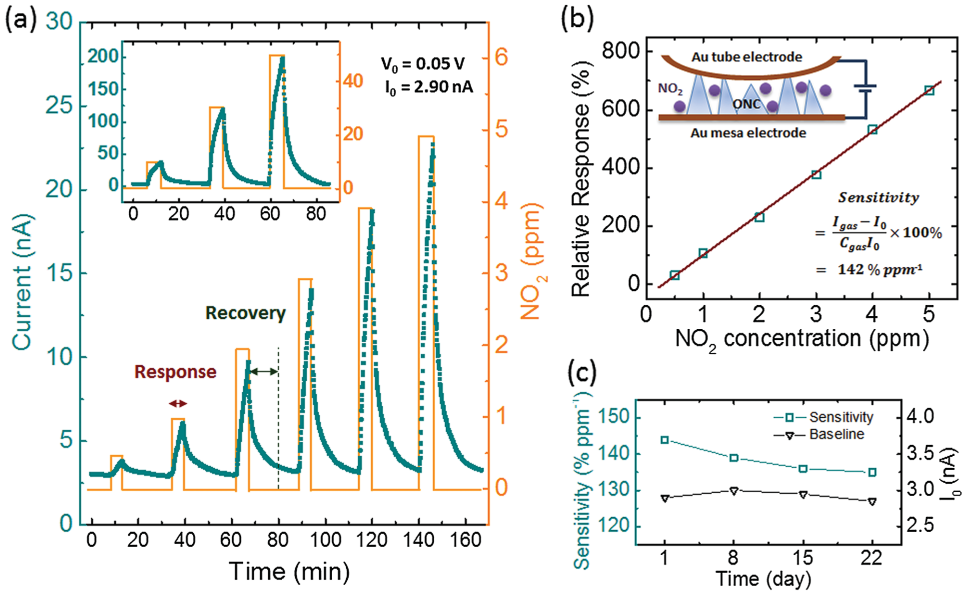

Figure 4. Organic nanocrystal diode sensor performance with respect to NO_2 detection. a) Response of device 1 to periodic NO_2 exposure. Device is operated under 0.05 V bias applied to tube electrode. b) Relative response of sensor versus different NO_2 concentrations (from 0.5–5 ppm). c) Stability test of device 1 in ambient atmosphere: sensitivity (left axis) and baseline (right axis) over time.

is selected to detect NO_2 gas (up to 5 ppm) at RT, because it is of great importance to detect low concentrations of NO_2 for health protection and environment monitoring in general industry.[48] According to the charge transport results in Figure 3b, a voltage of +0.05 V well within the ohmic region is applied to the Au tube electrode. A stable constant current of about 2.90 nA is generated and used as the baseline for the sensing process. As presented in **Figure 4**a, the F_{16}CuPc/VOPc/F_{16}CuPc nanocrystal diode shows a good response and recovery behavior upon periodic exposure to NO_2 gaseous flow (200 standard cm^3 per minute (sccm)). After exposure to NO_2 the conduction of the diode increases instantaneously and the change in current is linear in concentration of the applied NO_2 at both low ppm level (Figure 4a) and up to 50 ppm (inset of Figure 4a). The sensing process consists of an initial fast response to the exposure and a much slower feedback signal at a later stage. The existence of these two stages is particularly evident when the concentration is beyond 10 ppm (inset of Figure 4a). The slow late response coincides with the typical saturation behavior in conventional inorganic gas sensors. However, the diffusion of gas molecules in organic materials causes the current to increase even after the sensing surfaces become saturated. Such phenomenon is widely found in gas sensors consisting of organic materials including graphene.[2,10,15,16,18,49,50] As shown in Figure 4a, we consider the first three minutes as the fast response stage, and define the current after a six minute exposure to NO_2 as the response current I_g. After ceasing the NO_2 flow, the diode conduction decreases correspondingly, and approaches the original current baseline I_0. The time after which 90% of the response current ($I_g - I_0$) is recovered, is defined as the recovery time of the gas sensor.

Another advantage of such nanoscale diodes is their large area-to-volume ratio, which is expected to be particularly sensitive to low density gas doses and very fast in electronic recovery. The nanocrystal diode was measured at various low-ppm levels (from 0.5 to 5 ppm) with good response. Based on these measurements, a relative response intensity, $S = \frac{I_g - I_0}{I_0} + 100\%$, was defined to describe the sensitivity, where I_0 is the baseline current, and I_g is the maximum current value after the exposure to NO_2 (response current, as defined above). As shown in Figure 4b, the relative response intensity which is taken from the highest current value of the sensing process for each gas dose, is a linear function of the NO_2 concentration, thus showing that the organic nanocrystal diode is well-behaved and works reliably at RT down to concentrations of 0.5 ppm. From the linear relationship, the slope which denotes the device sensitivity is determined to be 144% ppm^{-1} in the range from 0.5 to 5 ppm. For the high concentration range (10–50 ppm) the sensitivity is 140% ppm^{-1}. The investigation and optimization of the device sensing performance for ultralow concentrations (ppb level) and larger concentrations (more than 100 ppm) will be subject of future studies. Apart from the high sensitivity, a recovery time of about 12 min is extrapolated from the current decreasing process (Figure 4a). Compared to previous reports on RT organic NO_2 gas sensors,[14,16,17] the high sensitivity, and shorter recovery time in our work are predominantly ascribed to the firmly contacted ultracompact nanopyramid structures with large area-to-volume ratio. Few traps and grain boundaries reduce the probability of trapping gas molecules. Based on statistics of ten devices fabricated in parallel, the average sensitivity is 151% ppm^{-1} with a standard deviation of 14.3% ppm^{-1}, and the average baseline current is 2.89 nA with a standard deviation of 0.17 nA (Supporting Information, Table S1). The sensor performance of device 1 under 0.05 V is also measured under different gas flow. With increasing gas flow from 200 sccm up to 1000 sccm, the gas sensing behavior does not change significantly (Supporting Information, Figure S2). This indicates that the microtube electrode is stable enough to provide reliable

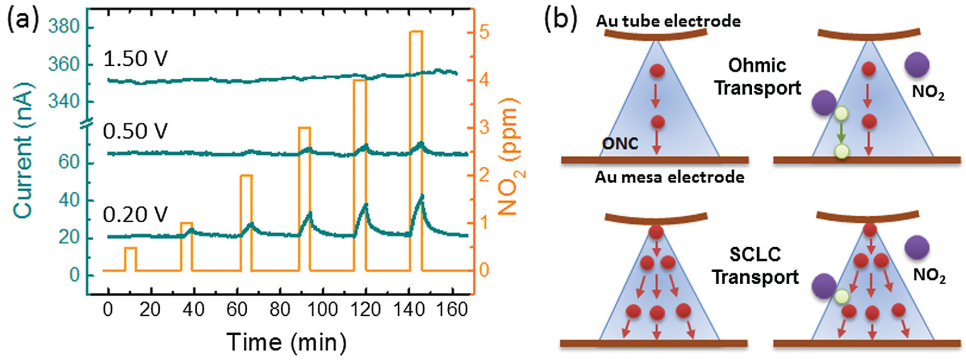

Figure 5. a) Response of organic nanocrystal diode sensor (device 1) under 0.20, 0.50, and 1.50 V bias applied to tube electrode. b) Schematic diagram of charge transport and response to NO_2 under Ohmic transport (upper panel) and SCLC transport (lower panel) conditions.

contact under certain gas flow, e.g. below 1000 sccm. Moreover, a long-term stability test was performed with the same device (device 1) shown in Figures 3 and 4a,b. The response performance to low ppm level NO_2 was measured over a time interval of more than three weeks. As shown in Figure 4c, owing to the good thermal and electronic stability of the VOPc material,[51] the device sensitivity only slightly decays from 144% ppm^{-1} to 135% ppm^{-1}, while the baseline remains constant at about 2.90 nA. Previously, metal phthalocyanines have shown detection limits down to 10 ppb NO_2 yet under heat treatment.[32] For RT NO_2 sensing based on organic thin films, detection limits of low ppm level (0.5–1 ppm) have been reported in several recent studies,[2,14,52] however, with slow recovery times. Our results demonstrate that cleverly designed nanostructured devices achieve fast recovery and reliable sensitive detection at low ppm level.

Furthermore, different transport modes occurring under certain biases are selected to detect the NO_2 gas. Voltages of +0.20, +0.50, and +1.50 V, which correspond to the transition from the ohmic to the SCLC region, are applied to the Au tube electrode of device 1. The response signals are monitored under periodic exposure to NO_2 (below 5 ppm). However, compared to the sensitive response current for +0.05 V, the response signals become weaker with increasing bias (**Figure 5**a). For example, the device is not able to detect NO_2 below 2 ppm at +0.50 V, and for +1.50 V, the device does not show any pronounced response behavior to the gas flow at all. The competition between the charge transport process and gas sensing mechanism is the major factor causing the different response result for low and high voltages. Within the ohmic range (Figure 5b upper panel), the current is in the range of nanoamperes or even less, and proportional to the applied voltage. When the nanocrystal diode is exposed to the analyte, extra carriers are provided by NO_2 apart from the limited amount of carriers injected from the tube electrode, resulting in an increased current in the output signal. Within the SCLC range (Figure 5b lower panel), the injected carriers reach an upper limit in the organic material for a certain applied voltage. As a result, the high concentration of injected carriers suppresses the charge generation from NO_2. It can be deduced that in SCLC mode NO_2 molecules are only physically absorbed on the organic nanocrystal and the charge exchange between the analyte and the organic is very weak. These interesting phenomena demonstrate that the organic nanocrystal diode provides a powerful platform to investigate the gas sensing mechanism at nanometer scale and offers new possibilities to develop advanced sensor devices.

Exploiting clever designs of nanostructure architectures for high performance devices is one of the major aims of nanomaterials research and nanotechnology. This work has demonstrated a facile fabrication and integration process for building functional organic devices based on nanoscale molecular structures and strain-engineered rolled-up metal nanomembranes. Nanodevices are often plagued by difficulties in contacting the nanostructured material and the interface between the metal electrode and organic material tends to limit the nano-device performance to a large extent. By utilizing efficient charge transfer in organic heterojunctions embedded in a vertical device geometry with ohmic contacts we are able to fully unleash the advantages of crystalline nanostructures. In particular, this includes their large area-to-volume ratio leading to a high average sensitivity of 151% ppm^{-1} and a fast recovery time (12 min) for a NO_2 sensor incorporating VOPc nanopyramids. As far as we know, this is the fastest organic semiconductor NO_2 sensor working at RT so far without any auxiliary treatments such as device heating and assisted reaction handling.[10,53]

Supporting Information

Supporting Information is available from the Wiley Online Library or from the author.

Acknowledgements

The authors acknowledge Martin Bauer, Wolfgang Borchardt, Paul Plocica, Bo Yu, Shiliang Ji, and Xiujin Wang for their technical support and helpful discussions. This research was financially supported by the Deutsche Forschungsgemeinschaft DFG Research Unit 1154 "Towards Molecular Spintronics," DFG Research Unit 1713 "Sensorische Mikro- and Nanosystme," and the National Natural Science Foundation of China (51330171).

Received: December 17, 2015
Revised: January 13, 2016
Published online: February 18, 2016

[1] L. Torsi, A. Dodabalapur, L. Sabbatini, P. G. Zambonin, *Sens. Actuator B: Chem.* **2000**, *67*, 312.
[2] M. I. Newton, T. K. H. Starke, M. R. Willis, G. McHale, *Sens. Actuator B: Chem.* **2000**, *67*, 307.
[3] B. Crone, A. Dodabalapur, A. Gelperin, L. Torsi, H. E. Katz, A. J. Lovinger, Z. Bao, *Appl. Phys. Lett.* **2001**, *78*, 2229.
[4] A. Das, R. Dost, T. Richardson, M. Grell, J. J. Morrison, M. L. Turner, *Adv. Mater.* **2007**, *19*, 4018.
[5] J. Huang, J. Miragliotta, A. Becknell, H. E. Katz, *J. Am. Chem. Soc.* **2007**, *129*, 9366.
[6] K. C. See, A. Becknell, J. Miragliotta, H. E. Katz, *Adv. Mater.* **2007**, *19*, 3322.
[7] L. Torsi, G. M. Farinola, F. Marinelli, M. C. Tanese, O. H. Omar, L. Valli, F. Babudri, F. Palmisano, P. G. Zambonin, F. Naso, *Nat. Mater.* **2008**, *7*, 412.
[8] T. Someya, A. Dodabalapur, J. Huang, K. C. See, H. E. Katz, *Adv. Mater.* **2010**, *22*, 3799.
[9] W. Huang, K. Besar, R. LeCover, A. M. Rule, P. N. Breysse, H. E. Katz, *J. Am. Chem. Soc.* **2012**, *134*, 14650.
[10] Y. Zang, F. Zhang, D. Huang, C.-A. Di, Q. Meng, X. Gao, D. Zhu, *Adv. Mater.* **2014**, *26*, 2862.
[11] P. T. Moseley, *Sens. Actuator B: Chem.* **1991**, *3*, 167.
[12] C.-A. Di, F. Zhang, D. Zhu, *Adv. Mater.* **2013**, *25*, 313.
[13] C. Zhang, P. Chen, W. Hu, *Chem. Soc. Rev.* **2015**, *44*, 2087.
[14] N. Padma, A. Joshi, A. Singh, S. K. Deshpande, D. K. Aswal, S. K. Gupta, J. V. Yakhmi, *Sens. Actuator B: Chem.* **2009**, *143*, 246.
[15] S. Ji, X. Wang, C. Liu, H. Wang, T. Wang, D. Yan, *Org. Electron.* **2013**, *14*, 821.
[16] S. Ji, H. Wang, T. Wang, D. Yan, *Adv. Mater.* **2013**, *25*, 1755.
[17] X. Wang, S. Ji, H. Wang, D. Yan, *Sens. Actuator B: Chem.* **2011**, *160*, 115.
[18] Y. Sadaoka, T. A. Jones, G. S. Revell, W. Göpel, *J. Mater. Sci.* **1990**, *25*, 5257.
[19] J. Huang, J. Sun, H. E. Katz, *Adv. Mater.* **2008**, *20*, 2567.
[20] G. Zhao, H. Dong, L. Jiang, H. Zhao, X. Qin, W. Hu, *Appl. Phys. Lett.* **2012**, *101*, 103302.
[21] L. Li, P. Gao, M. Baumgarten, K. Müllen, N. Lu, H. Fuchs, L. Chi, *Adv. Mater.* **2013**, *25*, 3419.
[22] T. Shaymurat, Q. Tang, Y. Tong, L. Dong, Y. Liu, *Adv. Mater.* **2013**, *25*, 2269.
[23] P. Guo, G. Zhao, P. Chen, B. Lei, L. Jiang, H. Zhang, W. Hu, M. Liu, *ACS Nano* **2014**, *8*, 3402.
[24] H. Haick, D. Cahen, *Acc. Chem. Res.* **2008**, *41*, 359.
[25] R. L. McCreery, A. J. Bergren, *Adv. Mater.* **2009**, *21*, 4303.
[26] R. M. Metzger, *Chem. Rev.* **2015**, *115*, 5056 .
[27] A. P. Bonifas, R. L. McCreery, *Nat. Nano* **2010**, *5*, 612.
[28] C. C. Bof Bufon, J. D. Arias Espinoza, D. J. Thurmer, M. Bauer, C. Deneke, U. Zschieschang, H. Klauk, O. G. Schmidt, *Nano Lett.* **2011**, *11*, 3727.
[29] C. C. S. Bof Bufon, J. D. Cojal González, D. J. Thurmer, D. Grimm, M. Bauer, O. G. Schmidt, *Nano Lett.* **2010**, *10*, 2506.
[30] C. C. Bof Bufon, C. Vervacke, D. J. Thurmer, M. Fronk, G. Salvan, S. Lindner, M. Knupfer, D. R. T. Zahn, O. G. Schmidt, *J. Phys. Chem. C* **2014**, *118*, 7272.
[31] T. A. Jones, B. Bott, *Sens. Actuator* **1986**, *9*, 27.
[32] B. Bott, T. A. Jones, *Sens. Actuator* **1984**, *5*, 43.
[33] H. Wang, Y. Zhou, V. A. L. Roy, D. Yan, J. Zhang, C.-S. Lee, *Org. Electron.* **2014**, *15*, 1586.
[34] S. Braun, W. R. Salaneck, M. Fahlman, *Adv. Mater.* **2009**, *21*, 1450.
[35] M. Grobosch, C. Schmidt, R. Kraus, M. Knupfer, *Org. Electron.* **2010**, *11*, 1483.
[36] J. Wang, H. Wang, X. Yan, H. Huang, D. Yan, *Appl. Phys. Lett.* **2005**, *87*, 093507.
[37] K. M. Lau, J. X. Tang, H. Y. Sun, C. S. Lee, S. T. Lee, D. Yan, *Appl. Phys. Lett.* **2006**, *88*, 173513.
[38] F. Zhu, H. Wang, D. Song, K. Lou, D. Yan, *Appl. Phys. Lett.* **2008**, *93*, 103308.
[39] H. Wang, Y. Donghang, *NPG Asia Mater.* **2010**, *2*, 69.
[40] K. Y. Law, *Chem. Rev.* **1993**, *93*, 449.
[41] H. Ohta, T. Kambayashi, K. Nomura, M. Hirano, K. Ishikawa, H. Takezoe, H. Hosono, *Adv. Mater.* **2004**, *16*, 312.
[42] H. Wang, D. Song, J. Yang, B. Yu, Y. Geng, D. Yan, *Appl. Phys. Lett.* **2007**, *90*, 253510.
[43] H. Wang, J. Wang, H. Huang, X. Yan, D. Yan, *Org. Electron.* **2006**, *7*, 369.
[44] X. Yan, J. Wang, H. Wang, H. Wang, D. Yan, *Appl. Phys. Lett.* **2006**, *89*, 053510.
[45] S. M. Yoon, S. J. Lou, S. Loser, J. Smith, L. X. Chen, A. Facchetti, T. Marks, *Nano Lett.* **2012**, *12*, 6315.
[46] K. C. Kao, W. Hwang, *Electrical Transport in Solids: With Particular Reference to Organic Semiconductors*, Pergamon, New York **1981**.
[47] F. Zhu, J. Yang, D. Song, C. Li, D. Yan, *Appl. Phys. Lett.* **2009**, *94*, 143305.
[48] *U. S. Occupational Safety and Health Standards, 1910.1000 TABLE Z-1*.
[49] W. Yuan, A. Liu, L. Huang, C. Li, G. Shi, *Adv. Mater.* **2013**, *25*, 766.
[50] J. C. Hsieh, C. J. Liu, Y. H. Ju, *Thin Solid Films* **1998**, *322*, 98.
[51] L. Wang, G. Liu, F. Zhu, F. Pan, D. Yan, *Appl. Phys. Lett.* **2008**, *93*, 173303.
[52] J. H. Shu, H. C. Wikle, B. A. Chin, *Sens. Actuator B: Chem.* **2010**, *148*, 498.
[53] M. Tiemann, *Chem. Eur. J.* **2007**, *13*, 8376.